Journal of Alloys and Compounds 586 (2014) 99–104

Contents lists available at ScienceDirect

Journal of Alloys and Compounds

journal homepage: www.elsevier.com/locate/jalcom

Graphene modulated assembly of PtPd bimetallic catalysts for electro-oxidation of methanol

Aiping Liu [a,b,c,*], Ming Yuan [a], Ming Zhao [a], Congda Lu [c], Tingyu Zhao [a], Peigang Li [a], Weihua Tang [d]

[a] Center for Optoelectronics Materials and Devices, Key Laboratory of Advanced Textile Materials and Manufacturing Technology, Ministry of Education, Zhejiang Sci-Tech University, Hangzhou 310018, China
[b] State Key Lab of Silicon Materials, Zhejiang University, Hangzhou 310027, China
[c] Key Laboratory of E&M (Zhejiang University of Technology), Ministry of Education & Zhejiang Province, Hangzhou 310032, China
[d] State Key Laboratory of Information Photonics and Optical Communication, Beijing University Posts and Telecommunications, Beijing 100876, China

ARTICLE INFO

Article history:
Received 24 August 2013
Received in revised form 8 October 2013
Accepted 9 October 2013
Available online 19 October 2013

Keywords:
Reduced graphene oxide
PtPd bimetallic catalyst
Electrocatalytic activity
Oxygen functionality
Fuel cell

ABSTRACT

Reduced graphene oxide-supported PtPd bimetallic nanoparticles (PtPd/rGO) were synthesized by the simple electrodeposition method and used as efficient catalysts for methanol electro-oxidation. The graphitization degree and oxygen functionalities of rGO sheets were adjusted by changing the reduction time of GO. Our results indicated that the moderately reduced rGO sheets on ITO substrates presented adequate oxygen functionalities as reactive sites for the nucleation and growth of bimetallic nanoparticles, which was helpful for improving the catalytic activity and stabilization of PtPd bimetallic nanoparticles on rGO. The PtPd/rGO hybrids showed lower onset potential and higher peak currents toward methanol oxidation than the PtPd bimetallic catalysts in the neutral media, highlighting the importance of rGO as the catalyst support for the potential application in fuel cells.

1. Introduction

Direct methanol fuel cells are identified as promising energy converters for a variety of portable applications due to the high energy-conversion efficiency, system simplicity, low pollution and environmental friendliness [1–3]. Consideration for the high cost, poisonous CO adsorbate poisoning and insufficient durability of the widely used Pt-based catalysts, other metals or metal oxides such as Au, Ru, Pd and Pb are often used to form metallic/alloyed catalysts to mitigate CO poisoning effect and pursue efficient catalysis [2–8] through a bifunctional or multifunctional mechanisms. Among the Pt-based alloyed catalysts, the PtPd bimetallic nanoparticles (NPs) may be potential candidates as catalysts of fuel cells because of the similarity of Pd with Pt for the oxygen reduction reaction, the lower cost and abundance of Pd [4,9–12]. However, these Pt-based metallic/alloyed catalysts frequently suffer from dissolution, sintering and agglomeration during operation of fuel cell, resulting in catalyst degradation [13]. To overcome this obstacle, nanostructured catalyst supports such as carbon (active carbon, porous carbon, carbon nanotube and graphene (GE)), carbide and conducting polymer have been developed to maximize the electroactive surface area of catalysts and improve their catalytic activity and durability [8–12,14–16]. Among these supports, the GE with a two-dimensional or three-dimensional nanostructure [2,17,18] is given great interest due to its potential application in lithium batteries, dye degradation, photocatalysts and supercapacitors [19–22]. Combination with its high surface area, high conductivity and low manufacturing cost, GE is regarded as a new-generation catalyst support because of its excellent chemical and environmental stability and strong adhesion to catalyst NPs, which provides better mass transport of reactants and electron transfer to the catalyst [23,24]. Recently, lots of research based on the synthesis of GE-supported metallic catalysts by using different methods and the modulation of catalytic behaviors by changing catalyst size, shape and components has been broadly reported [2,9–12,18–27]. The catalysts supported on the reduced graphene oxide (rGO) also show improved activity than those supported on carbon black [28]. However, the preparation of metal/GE nanocomposites in many studies uses the organic additives, surfactants or stabilizers to improve the compatibility of GE in the solvent, which might greatly damage the catalyst performance due to the strongly absorption of additives on the metal surfaces. The electrochemical method is regarded as green, simple and fast [10,18,25,29,30], which is suitable for the industrial production and large-area electrode fabrication without the use of additives. Furthermore, extensive studies have revealed that the structures

* Corresponding author at: Center for Optoelectronics Materials and Devices, Key Laboratory of Advanced Textile Materials and Manufacturing Technology, Ministry of Education, Zhejiang Sci-Tech University, Hangzhou 310018, China. Tel./fax: +86 571 86843468.
E-mail address: liuaiping1979@gmail.com (A. Liu).

0925-8388/$ - see front matter © 2013 Elsevier B.V. All rights reserved.
http://dx.doi.org/10.1016/j.jallcom.2013.10.070

and properties of carbon supports, including surface functional groups, graphitization degree and surface area, affect the activity and stability of the catalysts [23,24]. The oxygen-containing groups of rGO play an important role in increasing support–metal interactions and stabilizing the catalysts [23,31,32]. For example, He et al. demonstrated the adjusted electrochemical activity and stability of Pt/rGO catalysts by changing the oxygenated groups on the rGO surface [23]. Our previous results indicated that the reduction degree of rGO affected the oxygen functionalities at the rGO surface, namely the reactive sites for nucleation and growth of gold NPs [32]. Therefore, the controllable assembly of Pt-based bimetallic catalysts on the rGO supports with different reduction degrees should be further investigated to explore the effect of oxygen functionalities of rGO on the catalyst activity.

In this paper, the rGO-supported PtPd bimetallic NPs (PtPd/rGO) were synthesized by the simple and effective electrodeposition method (Fig. 1a), allowing bimetallic NPs uniformly anchored on the surfaces of rGO nanosheets. The effect of rGO reduction degree adjusted by the electrochemical reduction time on the nucleation and growth of PtPd NPs was studied. The PtPd/rGO composites as anode catalysts for methanol oxidation were investigated in detail (Fig. 1b).

2. Experimental

2.1. Reagents

Graphite power (50 μm) was purchased from Shanghai Carbon Co., Ltd. $H_2PtCl_6 \cdot 6H_2O$ (purity 99.99%) and $PdCl_2$ (purity 99.99%) were supplied by Sigma, USA. All other chemicals were of analytical grade and used without further purification. The water was obtained from a Millipore Q purification system (resistivity>18 MΩ cm).

2.2. Preparation of PtPd/rGO composites

A 0.5 mg/mL exfoliated GO aqueous solution was prepared by modified Hummers method [33] and was spin-coated on clean ITO surfaces at 4000 rpm for 30 s. The GO sheets with different thicknesses (about 2 nm and 5 nm) were further electrochemically reduced for 2 min or 10 min in a 20 mM KH_2PO_4 supporting electrolyte with the potential controlled from 0 to −1.5 V (*vs.* saturated calomel electrode, SCE) at 0.05 V/s. An electrochemical workstation (CHI 660B, USA) with GO/ITO working electrode, SCE reference electrode and platinum foil counter electrode was used. The as-prepared rGO/ITO electrodes were then immersed into a 0.5 M Na_2SO_4 solution containing 2 mM H_2PdCl_4 to electrodeposit Pd NPs on rGO/ITO surfaces at a constant voltage of −1.0 V (*vs.* SCE) for 400 s, followed by the electrodeposition of Pt NPs on the Pd/rGO/ITO surfaces with the potential controlled from 0 to −1.0 V (*vs.* SCE) at 0.05 V/s for 1600 s in a 0.5 M Na_2SO_4 solution containing 1 mM H_2PtCl_6. The weight loadings of PtPd NPs onto the rGO sheets were calculated by the integral areas related to Pd and Pt deposition in the electrochemical measurements. Besides, the Pd/ITO, Pt/ITO and PtPd/ITO specimens without the rGO supports were also fabricated as the references.

2.3. Characterization and measurements

The C 1s spectra of composites were obtained by X-ray photoemission spectroscopy (XPS, KRATOS AXIS ULTRA-DLD). The X-ray diffraction (XRD) patterns of different complex were collected on a diffractometer (Bruker AXS D8) using the Cu Kα radiation (λ = 0.15418 nm) with the 2θ scan from 5° to 90° at a step of 0.02°. The Raman spectra were acquired with a Thermo Fisher DXR Raman spectrometer using a He–Ne laser (λ = 632.8 nm). The morphologies and components of different composite electrodes were obtained by the scanning electron microscopy (SEM, Hitachi S4800) equipped with an energy-dispersive X-ray spectroscopy (EDS).

All electrochemical measurements were carried out on the CHI660B electrochemical workstation. The electrochemically active surface areas (ECSAs) of Pt and PtPd catalysts were calculated from hydrogen absorption curve recorded in a 0.5 M H_2SO_4 solution at a scan rate of 0.05 V/s by using the charge for monolayer adsorption/desorption of hydrogen on Pt (210 μC/cm^2) [34]. Since the hydrogen might diffuse into the Pd bulk to form Pd hydride rather than adsorb onto the Pd surface, the ECSA of Pd NPs was determined by the coulombic charge (4.05 C/m^2) for the reduction of palladium oxide monolayer [35]. The electrochemical behaviors of the $Fe(CN)_6^{3-/4-}$ redox couple at different electrodes were investigated in the 5 mM $K_3Fe(CN)_6$ and 1 M KCl mixed solution at different scan rates. Cyclic voltammogram (CV) and chronoamperometry (CA) measurements of different composite electrodes toward methanol oxidation were performed in a 0.5 M Na_2SO_4 solution containing 5 M methanol using the above three-electrode system. All electrolyte solutions were purged with high-purity nitrogen before electrochemical experiments at room temperature.

3. Results and discussion

3.1. Microstructures

Fig. 2a shows the CVs of electrochemical reduction of 5-nm GO on the ITO surface in a potential range from 0.0 to −1.5 V at 0.05 V/s. The large cathodic peak at about −1.1 V is attributed to the reduction of oxygen-containing groups of GO [36]. The reduction peak becomes weaker with the increasing reduction time and almost disappears after 10-min scanning (10 cycles). We usually determine the GO as slightly reduced one when the reduction peak current decreases to 60–70% (after 2-min scanning) of the prime one (the first cycle). When the reduction peak almost disappears and the current become stable after 10-min scanning (10 cycles), the GO is regarded as moderately reduced one. Further scanning does not result in the obvious decrease of current since only a few of oxygen functionalities are further reduced. Therefore, the GO is regarded as excessively reduced one after that. In like manner, the reduction peak almost disappears after 2-min scanning for

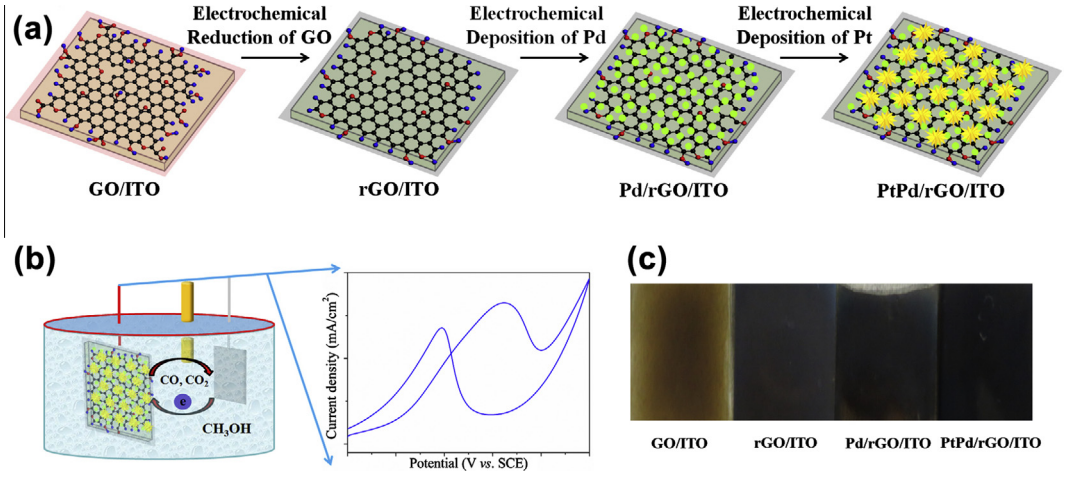

Fig. 1. Schematic illustrations of (a) the formation of PtPd/rGO/ITO electrode by an electrochemical method, (b) electrochemical detection for methanol oxidation on the PtPd/rGO/ITO electrode and (c) photo images of different electrodes.

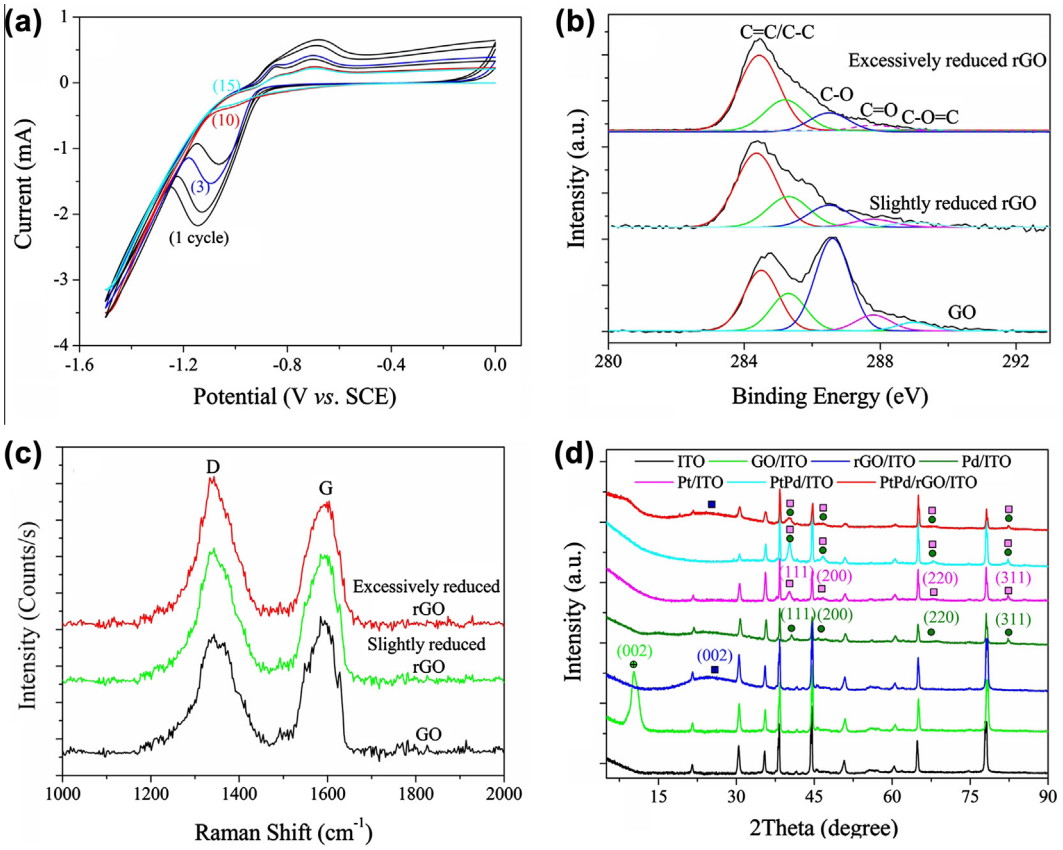

Fig. 2. (a) Cyclic voltammograms of electrochemical reduction of 5-nm GO on the ITO surface, (b) XPS curves fit of C 1s spectra of GO and rGO sheets, (c) Raman spectra of GO and rGO sheets and (d) XRD patterns of different samples.

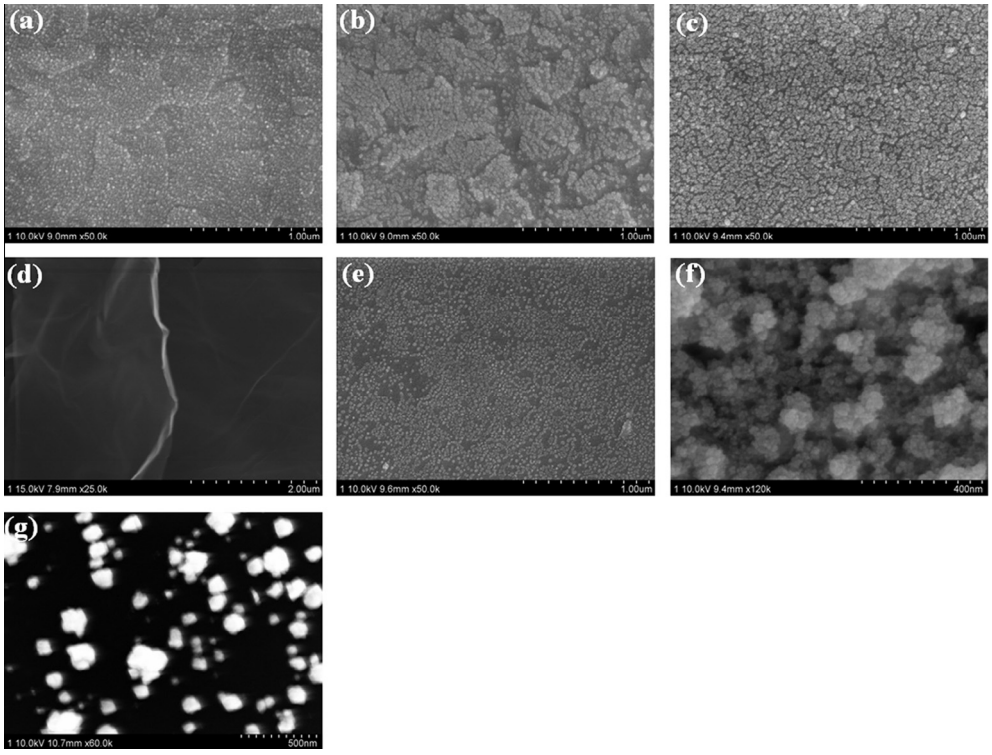

Fig. 3. Scanning electron microscopy images of (a) Pd/ITO, (b) Pt/ITO, (c) PtPd/ITO, (d) rGO/ITO, (e) Pd/rGO/ITO and (f) and (g) PtPd/rGO/ITO. The rGO sheets were (d) and (f) moderately and (g) excessively reduced, respectively.

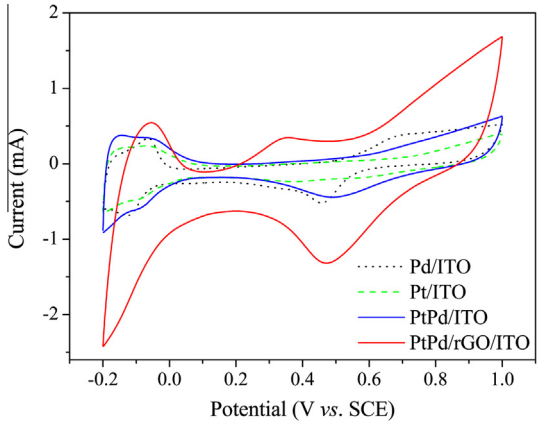

Fig. 4. Cyclic voltammograms of different electrodes in a N_2 saturated 0.5 M H_2SO_4 solution at a scan rate of 0.05 V/s. The rGO sheets were moderately reduced.

the 2-nm GO nanosheets. Therefore, the 2-nm GO sheets are regarded to be moderately and excessively reduced after 2-min and 10-min scannings, respectively. The color of GO/ITO sample changes from brown to black (Fig. 1c) after reduction, indicating the formation of rGO. Fig. 2b shows the C 1s fitting spectra of GO and rGO sheets. The five peaks at 284.4 ± 0.1 eV, 285.2 ± 0.1 eV, 286.5 ± 0.1 eV, 287.8 ± 0.1 eV and 289.0 ± 0.1 eV are corresponding to the C═C, C—C, C—O, C═O and O—C═O bonds [32,37], respectively. The peak associated with C—O is predominant for GO film and the atomic percentage of C/O increases from 1.74 for GO to 3.89 for slightly reduced rGO to 4.91 for excessively reduced rGO, demonstrating enhanced reduction degree from GO to rGO [32]. The higher intensity ratio of D peak (at 1340 cm^{-1}) to G peak (at 1590 cm^{-1}) for excessively reduced rGO also confirms its higher reduction degree with restored ordered structure after the electrochemical reduction [25,32,36] (Fig. 2c) due to the creation of new small-sp^2 domains [38]. This indicates that the rGO sheet with higher C/O atomic ratio shows higher graphitization degree. The XRD patterns of different samples are shown in Fig. 2d. The diffraction peak at $2\theta = 10.2°$ (GO/ITO) is attributed to the (002) facet of GO sheet, corresponding to a layer-to-layer distance (d-spacing) of about 0.87 nm. The peak moves to $2\theta = 25.7°$ after electrochemical reduction due to the intercalated water molecules elimination between neighboring rGO sheets [36]. The diffraction peaks at about $2\theta = 40.5°$, 46.8°, 68.2° and 82.4° for Pd and $2\theta = 40.1°$, 46.6°, 67.7° and 82.3° for Pt are corresponding to the (111), (200), (220) and (311) crystalline planes of face-centered cubic Pd (JCPDS No. 46-1043) and Pt (JCPDS No. 04-0802).

Fig. 3 shows the morphologies of Pd and Pt NPs electrodeposited on different substrates. The Pd and Pt NPs and the PtPd bimetallic NPs are uniformly dispersed on the ITO surface (Fig. 3a–c). The wrinkles of moderately reduced rGO sheets on ITO (Fig. 3d) may be important for preventing aggregation of rGO due to the van der Waals forces during drying and maintaining high surface area [28]. The Pd NPs anchored on the moderately reduced rGO/ITO surfaces show less aggregation with the uniform size about 15–20 nm (Fig. 3e). This is attributed to the oxygen functionalities with negative charges at the rGO surface which favor the Pd^{2+} adsorption on rGO and stabilize the Pd NPs with uniform size and excellent dispersion [10,23]. While the further removal of these oxygen-containing groups from rGO surface leads to a remarkable increase in Pd NP sizes due to the aggregation, indicating that the oxygen-containing groups on rGO surfaces do play an important role in enhancing the loading and dispersion of metal NPs [23,24,32]. Besides, the PtPd NPs on the moderately reduced rGO surface show a porous structure (Fig. 3f) due to the existent

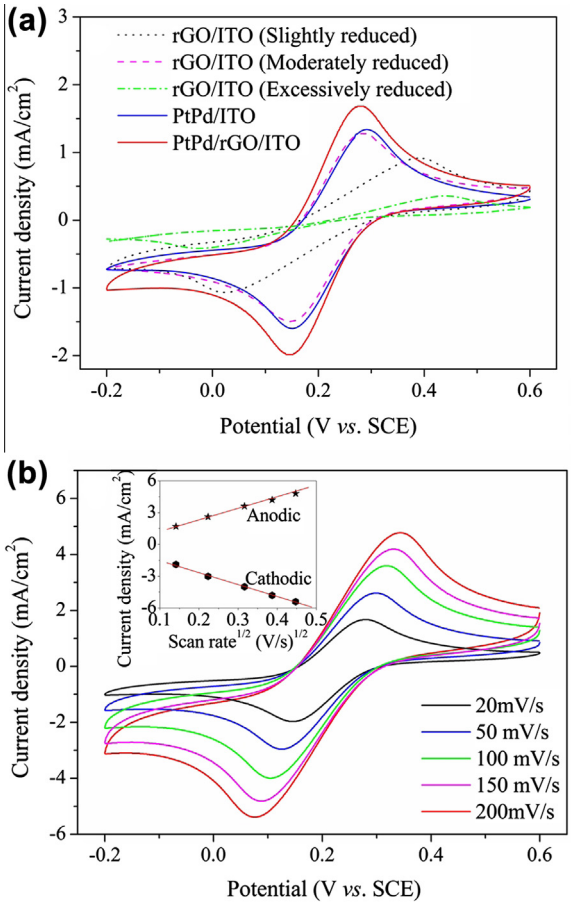

Fig. 5. Cyclic voltammograms of (a) different samples in a 1 M KCl solution including 5 mM $K_3Fe(CN)_6$ at a scan rate of 0.02 V/s and (b) moderately reduced PtPd/rGO/ITO in a 1 M KCl solution including 5 mM $K_3Fe(CN)_6$ at different scan rates. The inset is the relation of square root of scan rate and peak current density.

repulsion force between negative charged $[PtCl_6]^{4-}$ and negative charged oxygen functionalities at the rGO surface [23], providing a larger active surface compared to the PtPd NPs on ITO surface (Fig. 3c). The PtPd NPs loaded on the excessively reduced rGO surface show obviously aggregated (Fig. 3g). The weight loadings of PtPd NPs onto the moderately and excessively reduced rGO sheets are about 0.1 mg and 0.03 mg, respectively, in the contact areas about 1.5 cm × 2.0 cm. The atomic percentage of Pt to Pd in the PtPd and PtPd/rGO catalyst is determined to be 70/30 by EDS.

3.2. Electrochemical and electrocatalytic activities of PtPd/rGO complex

The CV curves obtained at different composite electrodes in a N_2 saturated 0.5 M H_2SO_4 solution at a scan rate of 0.05 V/s are shown in Fig. 4, which exhibit the typical hydrogen adsorption/desorption, double-layer and metal oxide formation/reduction characteristics [10,23]. The higher current response obtained on the PtPd/rGO/ITO electrode is attributed to its porous nanostructure. Furthermore, the $[Fe(CN)_6]^{3-/4-}$ couple is widely used as an electrochemical probe to evaluate the electrochemical active of materials. The GO is electrically insulating and full of defects. For the slightly reduced rGO, the oxygen functionalities on the rGO as the defects affect the fast transport of electron, resulting in a slower redox reaction and larger peak-to-peak potential separation (Fig. 5a) [23]. When GO is moderately reduced to rGO, the reconstruction of ordered carbon structure increases the electron trans-

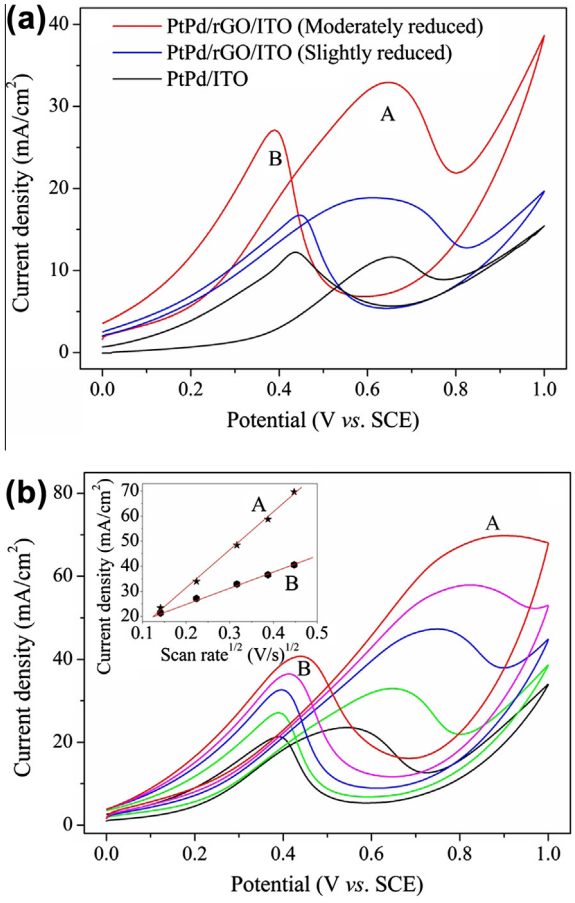

Fig. 6. Cyclic voltammograms of 5 M methanol oxidation on (a) different electrodes in a N_2 saturated 0.5 M Na_2SO_4 solution at 0.05 V/s and (b) moderately reduced PtPd/rGO/ITO electrodes in a N_2 saturated 0.5 M Na_2SO_4 solution at different scan rates. The inset is the relation of square root of scan rate and peak current density.

port of rGO [23], presenting a good electrical conductivity and attendant high current response to $[Fe(CN)_6]^{3-/4-}$ reaction. In contrast, the excessively reduced rGO with few oxygen functionalities does not display obvious electrochemical activity for $[Fe(CN)_6]^{3-/4-}$ reaction due to the PtPd NPs aggregation (Fig. 3g). Besides, the rGO also plays an important role in the modulation of electrochemical activity of composite electrodes. The redox current response obtained at the moderately reduced PtPd/rGO modified electrode is larger than that obtained at the PtPd modified one, indicating the larger concentration gradients obtained in the porous metal deposits on rGO support. The CV curves of $[Fe(CN)_6]^{3-/4-}$ couple reaction at the moderately reduced PtPd/rGO/ITO electrode at different scan rates are recorded (Fig. 5b) and the anodic and cathodic peak currents increase linearly with the square root of scan rate (the inset of Fig. 5b), indicating the electrochemical reaction controlled by the semi-infinite linear diffusion from the electrolyte to the electrode.

Fig. 6 shows the CVs of methanol oxidation at different electrodes in a N_2 saturated 0.5 M Na_2SO_4 solution containing 5 M methanol at a scan rate of 0.05 V/s. All current densities are normalized with respect to the ECSAs. The first oxidation peak A observed at 0.65 V for PtPd/ITO in the positive scan (Fig. 6a) is assigned to the oxidation of methanol. In the backward scan, an oxidation peak B at around 0.45 V is observed. Goodenough et al. attributed this oxidation peak in the reverse scan to the removal of the incompletely oxidized carbonaceous species (Pt=C=O bonded on the Pt surface) in the forward scan [39]. Hence the ration of the forward anodic peak current density (I_f) to the reverse

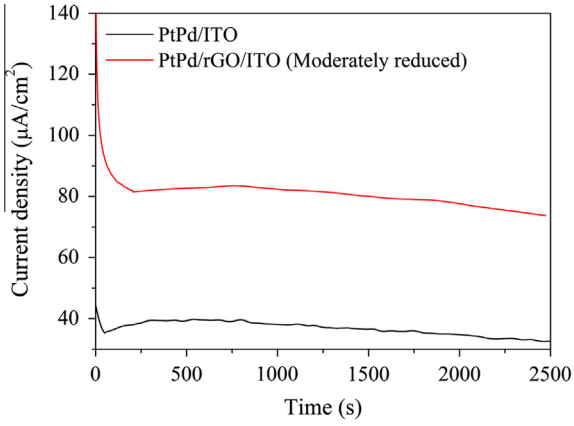

Fig. 7. Chronoamperometric curves for 5 M methanol oxidation on different electrodes in a N_2 saturated 0.5 M Na_2SO_4 solution at 0.35 V.

one (I_b) could be used to describe the catalyst tolerance to species accumulated on the electrode surface. The higher I_f/I_b ratio for the methanol oxidation suggests the higher tolerance to carbonaceous intermediate poisoning and higher oxidation activity of methanol. Furthermore, the rGO affects the catalytic activity of bimetallic catalysts (Fig. 6a). The more negative onset potential for the methanol oxidation on PtPd/rGO catalysts exhibits their superior catalytic activities toward methanol oxidation than PtPd one. The oxidation peak signals of A and B obtained at the moderately reduced PtPd/rGO catalyst are obviously higher than those obtained at PtPd bimetallic catalyst with the I_f/I_b ratio about 1.5 times higher than that of PtPd catalyst. This suggests that the moderately reduced rGO supported catalyst possesses better poison tolerance. This could be ascribed to the residual oxygen-containing groups on the moderately reduced rGO as binding sites of PtPd NPs, which favor the dispersion and stability of bimetallic catalyst with high ECSA and surface roughness. The oxygen-containing groups (such as OH) might also promote the oxidation of CO adsorbed on the active Pt sites and benefit the regeneration of Pt [40,41]. On the other hand, the ordered graphitization structure of rGO can facilitate electron transport and accelerate the mass transfer kinetics at the electrode surface, resulting in the increase in oxidation current [23]. The I_f and I_b for the moderately reduced PtPd/rGO catalysts are proportional to the square root of scan rate, suggesting the speedy diffusion-controlled procession for the fuel oxidation (Fig. 6b) [8,11]. However, the slightly reduced rGO with significant amount of oxygen-containing groups and excessively reduced rGO with few oxygen-containing groups and metal binding sites present weakened catalytic activity for methanol oxidation.

The CA curves for methanol oxidation on PtPd/ITO and moderately reduced PtPd/rGO/ITO electrodes are shown in Fig. 7. The high oxidation current obtained at the PtPd/rGO/ITO electrode decreases quickly and becomes stable after 250 s, indicating the higher catalytic activity and stability of the electrode. Therefore, a reasonable adjusting for the graphitization degree and oxygen-containing groups of rGO is important for the performance optimization of rGO supported bimetallic catalysts with high activity and stability.

4. Conclusions

The reduced graphene oxide (rGO) supported PtPd bimetallic catalyst was fabricated by a simple electrodeposition method. The surface oxygen-containing groups of rGO were beneficial for improving bimetallic nanoparticle dispersion on the rGO with restored ordered structure, giving the PtPd/rGO catalysts higher catalytic activity toward methanol oxidation compared to the PtPd

catalysts. Furthermore, the PtPd/rGO with moderately reduced rGO exhibited higher oxidation current density for methanol oxidation and better tolerance to CO absorption in the neutral media than those with slightly or excessively reduced rGO, indicating the importance of reasonable modulation for the graphitization degree and oxygen-containing groups of rGO to optimize the performance of fuel cells.

Acknowledgements

This work was supported by the National Natural Science Foundation of China (Nos. 51272237, 61274017 and 51175472), the Visiting Scholars Fund of State Key Lab of Silicon Materials, Zhejiang University (SKL2011-20), the Qianjiang Talent Program of Zhejiang Province (QJD1102007), the China Postdoctoral Science Foundation (Nos. 2012M520063, 2013T60587 and Bsh1201016), the Scientific Research Foundation for the Returned Overseas Chinese Scholars (State Education Ministry) and the Technology Foundation for Selected Overseas Chinese Scholar of China.

References

[1] C.Y. Wang, Chem. Rev. 104 (2004) 4727–4766.
[2] X.G. Wang, B. Tang, X.B. Huang, Y. Ma, Z.H. Zhang, J. Alloys Comp. 565 (2013) 120–126.
[3] Z.Y. Lv, Y. Fei, W.Y. Chen, Y.F. Tan, C.Q. Sun, J.R. Chen, A.J. Wang, J.J. Feng, J. Alloys Comp. 581 (2013) 717–723.
[4] S.J. Guo, S.J. Dong, E.K. Wang, Chem. Commun. 46 (2010) 1869–1871.
[5] Z.L. Liu, X.Y. Ling, X.D. Su, J.Y. Lee, J. Phys. Chem. B 108 (2004) 8234–8240.
[6] C. Medard, M. Lefevre, J.P. Dodelet, F. Jaouen, G. Lindbergh, Electrochim. Acta 51 (2006) 3202–3213.
[7] L.J. Zhang, Z.Y. Wang, D.G. Xia, J. Alloys Comp. 426 (2006) 268–271.
[8] L.F. Dong, R.R.S. Gari, Z. Li, M.M. Craig, S.F. Hou, Carbon 48 (2010) 781–787.
[9] S.J. Guo, S.J. Dong, E.K. Wang, ACS Nano 4 (2010) 547–555.
[10] X. Yang, Q.D. Yang, J. Xu, C.S. Lee, J. Mater. Chem. 22 (2012) 8057–8062.
[11] Y.Z. Zhang, Y.E. Gu, S.X. Lin, J.P. Wei, Z.H. Wang, C.M. Wang, Y.L. Du, W.C. Ye, Electrochim. Acta 56 (2011) 8746–8751.
[12] C.G. Hu, H.H. Cheng, Y. Zhao, Y. Hu, Y. Liu, L.M. Dai, L.T. Qu, Adv. Mater. 24 (2012) 5493–5498.
[13] Y.J. Wang, D.P. Wilkinson, J.J. Zhang, Chem. Rev. 111 (2011) 7625–7651.
[14] I.D. Choi, H. Lee, Y.B. Shim, D. Lee, Langmuir 26 (2010) 11212–11216.
[15] B. Liu, H.Y. Li, L. Die, X.H. Zhang, Z. Fan, J.H. Chen, J. Power Sources 186 (2009) 62–66.
[16] F. Alcaide, G. Alvarez, P.L. Cabot, H.-J. Grande, O. Miguel, A. Querejeta, Int. J. Hydrogen Energy 36 (2011) 4432–4439.
[17] Y.Q. Sun, Q.O. Wu, G.Q. Shi, Energy Environ. Sci. 4 (2011) 1113–1132.
[18] T. Maiyalagan, X.C. Dong, P. Chen, X. Wang, J. Mater. Chem. 22 (2012) 5286–5290.
[19] W. Xiao, Z.X. Wang, H.J. Guo, Y.H. Zhang, Q. Zhang, L. Gan, J. Alloys Comp. 560 (2013) 208–214.
[20] D.B. Lu, Y. Zhang, S.X. Lin, L.T. Wang, C.M. Wang, J. Alloys Comp. 579 (2013) 336–342.
[21] M. Ahmad, E. Ahmed, Z.L. Hong, N.R. Khalid, W. Ahmed, A. Elhissi, J. Alloys Comp. 577 (2013) 717–727.
[22] Z. Wang, C.Y. Ma, H.L. Wang, Z.H. Liu, Z.P. Hao, J. Alloys Comp. 552 (2013) 486–491.
[23] D.P. He, K. Cheng, T. Peng, X.L. Sun, M. Pan, S.C. Mu, J. Mater. Chem. 22 (2012) 21298–21304.
[24] G. Goncalves, P. Marques, C.M. Granadeiro, H.I.S. Nogueira, M.K. Singh, J. Gracio, Chem. Mater. 21 (2009) 4796–4802.
[25] Y.G. Zhou, J.J. Chen, F.B. Wang, Z.H. Sheng, X.H. Xia, Chem. Commun. 46 (2010) 5951–5953.
[26] Y.M. Li, L.H. Tang, J.H. Li, Electrochem. Commun. 11 (2009) 846–849.
[27] H.J. Yin, H.J. Tang, D. Wang, Y. Gao, Z.Y. Tang, ACS Nano 6 (2012) 8288–8297.
[28] R. Kou, Y.Y. Shao, D.H. Wang, M.H. Engelhard, J.H. Kwak, J. Wang, V.V. Viswanathan, C.M. Wang, Y.H. Lin, Y. Wang, I.A. Aksay, J. Liu, Electrochem. Commun. 11 (2009) 954–957.
[29] Y.Y. Shao, J. Wang, M. Engelhard, C.M. Wang, Y.H. Lin, J. Mater. Chem. 20 (2010) 743–748.
[30] S. Liu, J.Q. Wang, J. Zeng, J.F. Ou, Z.P. Li, X.H. Liu, S.R. Yang, J. Power Sources 195 (2010) 4628–4633.
[31] F. Coloma, A. Sepulveda-Escribano, J.L.G. Fierro, F. Rodriguez-Reinoso, Appl. Catal. A-Gen. 150 (1997) 165–183.
[32] A.P. Liu, T. Xu, Q.H. Ren, M. Yuan, W.J. Dong, W.H. Tang, Electrochem. Commun. 25 (2012) 74–78.
[33] W.S. Hummers, R.E. Offeman, J. Am. Chem. Soc. 80 (1958) 1339.
[34] M. Umeda, M. Kokubo, M. Mohamedi, I. Uchida, Electrochim. Acta 48 (2003) 1367–1374.
[35] Y.H. Qin, H.H. Yang, X.S. Zhang, P. Li, C.A. Ma, Int. J. Hydrogen Energy 35 (2010) 7667–7674.
[36] H.L. Guo, X.F. Wang, Q.Y. Qian, F.B. Wang, X.H. Xia, ACS Nano 3 (2009) 2653–2659.
[37] A.P. Liu, E.J. Liu, G.C. Yang, N.W. Khun, W.G. Ma, Pure Appl. Chem. 82 (2010) 2217–2229.
[38] S. Stankovich, D.A. Dikin, R.D. Piner, K.A. Kohlhaas, A. Kleinhammes, Y. Jia, Y. Wu, S.T. Nguyen, R.S. Ruoff, Carbon 45 (2007) 1558–1565.
[39] R. Manoharan, J.B. Goodenough, J. Mater. Chem. 2 (1992) 875–887.
[40] Z.Y. Ji, G.X. Zhu, X.P. Shen, H. Zhou, C.M. Wu, M. Wang, New J. Chem. 36 (2012) 1774–1880.
[41] S. Sharma, A. Ganguly, P. Papakonstantinou, X.P. Miao, M.X. Li, J.L. Hutchison, M. Delichatsios, S. Ukleja, J. Phys. Chem. C 114 (2010) 19459–19466.